Tunneling Processes into Localized Subgap States in Superconductors

Michael Ruby,[1] Falko Pientka,[2] Yang Peng,[2] Felix von Oppen,[2] Benjamin W. Heinrich,[1] and Katharina J. Franke[1]
[1]Fachbereich Physik, Freie Universität Berlin, 14195 Berlin, Germany
[2]Dahlem Center for Complex Quantum Systems and Fachbereich Physik, Freie Universität Berlin, 14195 Berlin, Germany
(Received 27 February 2015; published 20 August 2015)

We combine scanning-tunneling-spectroscopy experiments probing magnetic impurities on a superconducting surface with a theoretical analysis of the tunneling processes between (superconducting) tip and substrate. We show that the current through impurity-induced Shiba bound states is carried by single-electron tunneling at large tip-substrate distances and Andreev reflections at smaller distances. The single-electron current requires relaxation processes, allowing us to extract information on quasiparticle transitions and lifetimes.

DOI: 10.1103/PhysRevLett.115.087001 PACS numbers: 74.50.+r, 05.60.Gg, 74.25.F-, 74.55.+v

Introduction.—Impurity-induced subgap states provide a fruitful window into conventional and unconventional superconductors [1–3]. The Yu-Shiba-Rusinov states [4–6] bound by magnetic impurities in conventional s-wave superconductors are a simple model system for nonmagnetic impurity resonances in unconventional superconductors, probe the competition between superconducting and Kondo correlations [7–9], and might provide a platform for engineering topological superconducting phases with Majorana end states [10–13].

In scanning-tunneling spectroscopy, Shiba states induce resonances which occur symmetrically at positive- and negative-bias voltages [2,3,7,14]. Given their subgap nature, it is natural to describe the current into Shiba states as carried by Andreev processes. These processes transfer a Cooper pair into the condensate and are resonantly enhanced by the Shiba state [15–18]. Nevertheless, scanning-tunneling microscopy (STM) experiments on Shiba states are typically analyzed in terms of the tunneling density of states which is appropriate for single-electron tunneling [1,19,20]. This allows one to understand the observed asymmetry in height between the positive- and negative-bias peaks while Andreev processes would necessarily be symmetric in bias (for normal-state tips) [18].

Here, we combine scanning-tunneling microscopy and spectroscopy of Shiba states using superconducting tips with a comprehensive theoretical analysis to elucidate the nature of the tunneling processes. We show that both single-electron and Andreev tunneling contribute in experiments and explain the observed inversion of peak-height asymmetry as a function of tunneling rates. Our analysis shows that STM experiments on Shiba states provide access to quasiparticle relaxation rates in superconductors, complementing recent work on superconducting quantum dots [21–23] and Josephson junctions [24–27].

Experiments.—We have performed STM experiments probing Mn adatoms on a Pb(111) single crystal surface. The experiments were carried out with a SPECS JT-STM at the base temperature of 1.2 K as well as at 4.8 K. The Pb single crystal surface was cleaned by repeated sputter-anneal cycles until a clean, atomically flat, and superconducting surface was obtained (critical temperature $T_c = 7.2$ K and gap $\Delta = 1.35$ meV at 1.2 K). Mn adatoms were evaporated onto the clean sample at a temperature below 10 K, resulting in a density of 30 atoms per 100×100 nm^2 (see the Supplemental Material [28]). Our STM experiments were carried out with a Pb-covered, superconducting tip (see Ref. [7] for the preparation procedure) which improves resolution far beyond the Fermi-Dirac limit [30,31].

Figure 1 shows spectra of the differential conductance dI/dV as a function of sample bias V, acquired at various tip-sample distances and thus tunneling strengths with the tip placed above a Mn adatom. All spectra share the same characteristic peaks [32] but their intensities (normalized to the normal-state conductance) depend strongly on the tunneling strength and the sign of the bias voltage.

The peaks in the dI/dV spectra appear at thresholds for various fundamental tunneling processes between a superconducting tip and a superconducting substrate with a magnetic adatom. (i) Single electrons can tunnel when the negative-energy quasiparticle continuum of the tip overlaps with the positive-energy continuum of the substrate (or vice versa). This requires a threshold voltage $eV = \pm 2\Delta$. (ii) Thermally excited quasiparticles (holes) in the positive-(negative-) energy quasiparticle continuum induce a single-particle current even near zero bias. (iii) With a Shiba state of energy ϵ_0, a single-particle current flows when the negative-energy continuum of the tip overlaps with the Shiba state, or the positive-energy continuum with the symmetric energy $-\epsilon_0$. These processes have threshold biases $eV = \pm(\Delta + \epsilon_0)$. (iv) Because of thermal occupation, a single-electron current can also flow when the positive-energy continuum overlaps with the Shiba state (and symmetrically when the negative-energy continuum overlaps with $-\epsilon_0$). This requires a threshold bias

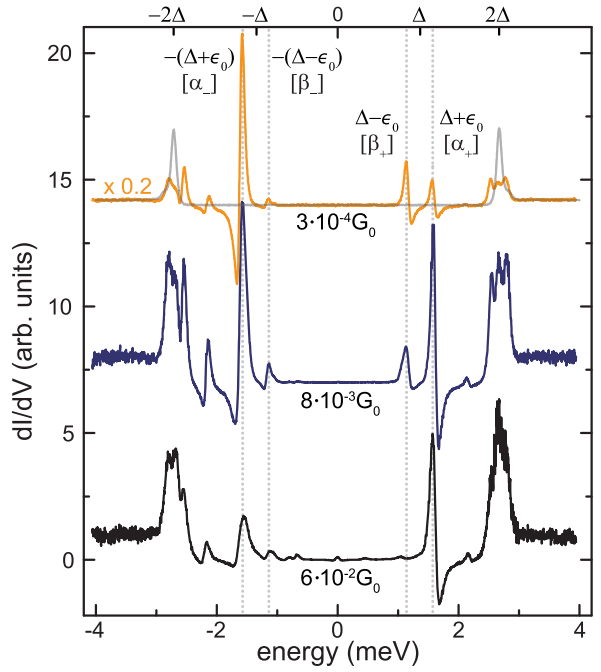

FIG. 1 (color online). dI/dV spectra measured on an isolated Mn adatom on Pb(111) for increasing tunneling strength from top to bottom (recorded with a lock-in modulation amplitude of 15 μV_{rms} at a frequency of 912 Hz). Spectra are normalized to the "normal-state" conductance measured at 4 meV (i.e., well outside the superconducting gap) in units of $G_0 = 2e^2/h$, offset for clarity and scaled when indicated for better visibility. The distance to the closest neighboring Mn atom was larger than 5 nm. A spectrum acquired above the clean Pb(111) surface overlays the smallest-conductance trace (top curve) for comparison. The four peaks originating from the deepest Shiba level are marked by dashed lines at $e|V| = \pm(\Delta \pm \epsilon_0)$.

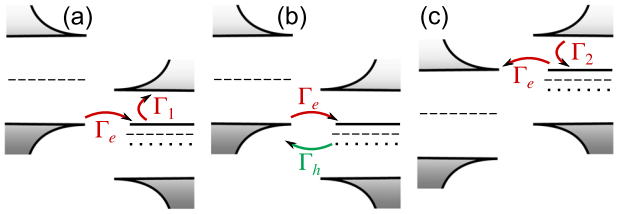

FIG. 2 (color online). Principal tunneling processes involving a Shiba state (solid line) within the superconducting gap (enclosed by BCS quasiparticle peaks). The chemical potential is represented by a dashed line. (a) Single-electron tunneling from tip to substrate [rate $\Gamma_e(\omega)$] with subsequent relaxation from the Shiba state to the quasiparticle continuum (rate Γ_1). (b) Andreev process transferring a Cooper pair to the substrate by electron and hole tunneling [with rates $\Gamma_e(\omega)$ and $\Gamma_h(\omega)$, respectively]. The processes in (a) and (b) both contribute near the threshold $eV = \Delta + \epsilon_0$. (c) Single-electron tunneling from substrate to tip [with rate $\Gamma_e(\omega)$] after occupation of the Shiba state by the relaxation of a thermal quasiparticle (with rate Γ_2), contributing to the thermal peak at $eV = -(\Delta - \epsilon_0)$. The current at the other two thresholds $eV = -(\Delta + \epsilon_0)$ and $eV = \Delta - \epsilon_0$ is carried by analogous hole processes (see the Supplemental Material [28]).

$eV = \pm(\Delta - \epsilon_0)$. (v) At $e|V| < 2\Delta$, an electron from, say, the tip can be reflected as a hole, transferring a Cooper pair. As all tunneling electrons and holes gain an energy eV, (multiple) Andreev processes between the quasiparticle continua have thresholds $eV = \pm 2\Delta/n$, with $n = 2, 3, \ldots$. Andreev processes require two or more particles to cross the tunnel barrier and thus become relevant for strong tunnel coupling only [33]. (vi) Shiba states induce additional *resonant* Andreev processes which become relevant at much lower tunneling rates. An electron from the negative-energy continuum of the tip can virtually tunnel into the Shiba state, reflect as a hole, and resonantly transfer a Cooper pair into the condensate of the substrate. Together with a similar process at reverse bias, this leads to thresholds at $eV = \pm(\Delta + \epsilon_0)$ which *coincide* with those for the single-electron processes. The principal tunneling processes involving the Shiba states are sketched in Fig. 2.

There is an important difference between the single-electron and resonant Andreev processes [18]. Single-electron processes change the occupation of the Shiba state, while Andreev processes merely transfer Cooper pairs into the condensate. Thus, a continuous current flow by single-electron processes requires relaxation processes which empty the Shiba state after it is occupied from the tip (or occupy the empty Shiba state); see Fig. 2. At finite temperature, a quasiparticle in the Shiba state can be excited to the continuum by absorption of a phonon or a photon (with rate Γ_1). Conversely, a thermally excited quasiparticle can relax into the Shiba state by emission (with rate Γ_2).

The observed peaks in the dI/dV spectra can now be correlated with Shiba states of energy $\simeq$0.22, $\simeq$0.77, and $\simeq$1.18 meV, respectively. The multiple Shiba states may reflect different angular-momentum channels or spin states $S > 1/2$ [14,34,35]. To analyze the tunneling processes, we focus on the most intense Shiba state at $\epsilon_0 \simeq 0.22$ meV. This state not only leads to the two *main* peaks at $eV = \pm(\Delta + \epsilon_0)$ (with peak height $\alpha_\pm$), but also to two pronounced *thermal* peaks at $eV = \pm(\Delta - \epsilon_0)$ (with peak height $\beta_\pm$). As it is the deepest state, its theoretical interpretation turns out to be least affected by the presence of the other Shiba states.

The heights of the peaks associated with this Shiba state are plotted in Fig. 3(a) over several decades in normal-state tunneling conductance. We draw attention to two important features of these data. First, the peak heights vary linearly over a wide region before turning sublinear at larger tunneling rates. Second, the asymmetry in the peak heights $\alpha_\pm$ between positive and negative biases inverts as a function of tunneling strength: At small tunneling rates, $\alpha_+ < \alpha_-$, while at large tunneling rates, $\alpha_+ > \alpha_-$. It is also evident that the inversion of the peak heights occurs at the crossover between the linear and sublinear regimes.

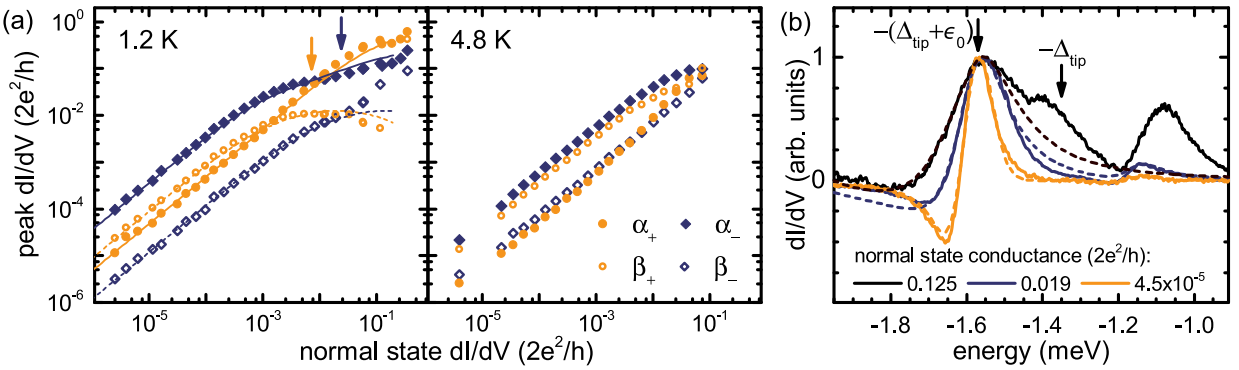

FIG. 3 (color online). (a) Peak heights $\alpha_\pm$ and $\beta_\pm$ of the four resonances associated with the deepest Shiba level (marked by dashed lines in Fig. 1) as a function of normal-state conductance at $T = 1.2$ K (left panel) and $T = 4.8$ K (right panel). The full (dashed) lines are fits to Eqs. (1) and (2) for the main (thermal) peaks. The crossover points between single-electron and Andreev contributions to $\alpha_\pm$ are indicated by arrows. (b) Experimental dI/dV traces of the Shiba peak near $eV = -(\Delta + \epsilon_0) \simeq -1.57$ meV at different junction conductances (solid lines). The spectra are normalized to the peak maximum. The dashed lines are theoretical fits of the Shiba peaks excluding multiple Andreev reflections.

Theoretical analysis.—It is often assumed [1] that the peak heights at positive and negative biases measure the electron and hole components u and v of the Shiba wave function. The observed inversion of peak heights implies that this cannot hold, in general. To gain further insight, we calculate the subgap current theoretically by a standard Keldysh calculation [36–38] (see the Supplemental Material for details [28]). Here, we focus on the physics underlying the results. Our calculation includes single-electron and Andreev processes involving the Shiba state as well as phenomenological rates Γ_1 and Γ_2 for relaxation processes between the Shiba state and the quasiparticle continuum. We neglect the nonresonant Andreev reflections at the superconducting tip (and thus multiple Andreev reflections [39]), which is justified except in the regime of very strong tunneling. With this approximation, the tunneling current becomes a sum of single-particle and Andreev currents, $I = I^s + I^a$, with

$$I^s = e\int \frac{d\omega}{2\pi\hbar}\left\{\frac{\Gamma_1[\Gamma_e n_F(\omega_-) - \Gamma_h n_F(\omega_+)]}{(\omega-\epsilon_0)^2+(\Gamma/2)^2} - \frac{\Gamma_2\{\Gamma_e[1-n_F(\omega_-)] - \Gamma_h[1-n_F(\omega_+)]\}}{(\omega-\epsilon_0)^2+(\Gamma/2)^2}\right\}, \quad (1)$$

$$I^a = 2e\int \frac{d\omega}{2\pi\hbar}\frac{\Gamma_h\Gamma_e[n_F(\omega_-) - n_F(\omega_+)]}{(\omega-\epsilon_0)^2+(\Gamma/2)^2}. \quad (2)$$

Here, the Fermi functions n_F are evaluated at $\omega_\pm = \omega \pm eV$ and $\Gamma = \Gamma_e + \Gamma_h + \Gamma_1 + \Gamma_2$.

The expressions for I^s and I^a can be understood in terms of the basic processes discussed above. The Andreev current I^a involves tunneling of an electron, described by $\Gamma_e(\omega) = 2\pi u^2\rho(\omega - eV)t^2$, and a hole, described by $\Gamma_h(\omega) = 2\pi v^2\rho(\omega + eV)t^2$. Here, t is the amplitude for tunneling between tip and substrate. The rates Γ_e and Γ_h are strongly ω dependent through the tip's BCS density of states $\rho(\omega)$. The denominator in Eq. (2) reflects the intermediate virtual occupation of the Shiba state. It includes the rates Γ_1 for depopulating the Shiba state by excitation to the continuum and Γ_2 for occupying the Shiba state by a thermally excited quasiparticle. The latter processes are assumed to be ω independent. The four contributions to the single-particle current I^s directly correspond to the peaks α_+ [term $\propto \Gamma_1\Gamma_e$; see Fig. 2(a)], α_- (term $\propto \Gamma_1\Gamma_h$), β_- [term $\propto \Gamma_2\Gamma_e$; see Fig. 2(c)], and β_+ (term $\propto \Gamma_2\Gamma_h$).

Equations (1) and (2) provide the following basic picture consistent with the data in Fig. 3(a): At weak tunneling, the relaxation rates Γ_1 and Γ_2 are faster than the tip-substrate tunneling. Once an electron tunnels into the Shiba state from the tip, it is rapidly excited to the quasiparticle continuum. In this regime, the tunnel current is dominated by the single-electron current I^s which is proportional to t^2, and thus to the normal-state conductance. The Andreev current I^a is a small correction scaling as t^4. This explains the wide linear regime in Fig. 3(a). At stronger tunneling, the tunneling rates become comparable to and eventually larger than the relaxation rates Γ_1 and Γ_2. Here, the t dependence of the broadening Γ leads to a sublinear or even a decreasing dependence of the peak heights on the normal-state conductance. As the relaxation processes are thermally activated, the crossover point between the linear and the sublinear regime is strongly temperature dependent, moving to lower normal-state conductances for lower temperatures. This is consistent with a comparison between the two panels of Fig. 3(a).

Linear regime.—This picture is substantiated by quantitatively analyzing the linear regime. At weak tunneling, the broadening is dominated by quasiparticle relaxation, $\Gamma \simeq \Gamma_1$ (for $\Gamma_1 \gg \Gamma_2$, i.e., $\epsilon_0 \gg T$). Then, Eq. (1) yields

$$\alpha_+ \sim \frac{2e^2}{h}\frac{\gamma_e\sqrt{\Delta}}{(\Gamma_1)^{3/2}}; \qquad \beta_- = \alpha_+\frac{\Gamma_2}{\Gamma_1} \tag{3}$$

for the peak heights [28]. Here, we introduced the normal-state electron (hole) tunneling rate $\gamma_e = 2\pi t^2\nu_0 u^2$ ($\gamma_h = 2\pi t^2\nu_0 v^2$), where ν_0 is the normal-state density of states of the tip. The expressions for α_- and β_+ simply differ by the substitution $u \leftrightarrow v$ (or $\gamma_e \leftrightarrow \gamma_h$). Thus, in this regime, the peak height is indeed a measure of the Shiba wave function at the tip position. From the data in Fig. 3(a), we extract $\alpha_+/\alpha_- = (u/v)^2 \approx 0.13$.

All four peaks are related by the relation $\alpha_+\beta_+ = \alpha_-\beta_-$. This is readily checked against the data in Fig. 3(a) and indeed, we find that this identity is well satisfied in the linear regime [28]. Moreover, the thermal and main peaks in Eq. (3) differ only by a ratio of relaxation rates, $\alpha_+/\beta_- = \Gamma_1/\Gamma_2 = \exp(\epsilon_0/T)$. Here, the last equality follows from detailed balance. This is in excellent agreement for the data at $T = 4.8$ K. At $T = 1.2$ K, we extract a slightly higher temperature of $T = 1.6$ K from the ratio of peak heights. Still, these considerations point to a relaxation process involving thermal activation rather than the quasiparticle bath suggested in Ref. [18].

Regime of strong tunneling.—At stronger tunneling, the broadening is dominated by tunneling, $\Gamma \simeq \Gamma_e + \Gamma_h$. Because of this broadening, the single-particle conductance reaches a maximum and eventually decreases with tunneling strength. As a result, the thermal peaks $\beta_\pm$ should exhibit a maximum vs normal-state conductance. The situation is different for the main peaks $\alpha_\pm$ with their additional Andreev contribution, which keeps increasing and eventually dominates the peak magnitude. Sufficiently far into this regime, Eqs. (1) and (2) yield

$$\alpha_+ \sim (2e^2/h)[\gamma_h\sqrt{\Delta/\epsilon_0}/(\gamma_e\sqrt{\Delta})^{2/3}], \tag{4}$$

$$\beta_- \sim (2e^2/h)[\Gamma_2/(\gamma_e\sqrt{\Delta})^{2/3}], \tag{5}$$

as well as α_- and β_+, which differ again by $u \leftrightarrow v$. The main peaks $\alpha_\pm$ keep increasing with tunneling $\gamma_{e,h}$, albeit with a sublinear dependence. The strong voltage dependence of the tunneling-induced broadening leads to a change in the line shape at strong tunneling. Indeed, we observe a vanishing of the negative differential conductance dip [see Fig. 3(b)] signaling the transition to the strong-tunneling regime [28].

Unlike for normal-metal tips [18,28], the Andreev contribution to the main peaks $\alpha_\pm$ is asymmetric for a superconducting tip, but with the asymmetry reversed relative to single-electron tunneling. While we have $\alpha_+/\alpha_- = (u/v)^2$ in the linear regime, Eq. (4) predicts $\alpha_+/\alpha_- = (v/u)^{10/3}$ in the Andreev-dominated regime. Indeed, an inversion of the peak heights $\alpha_\pm$ is seen in Fig. 3(a), as pointed out above.

Equation (5) predicts that the thermal peaks also invert, from $\beta_-/\beta_+ = (u/v)^2$ in the linear regime to $\beta_-/\beta_+ = (v/u)^{4/3}$ in the sublinear regime. This inversion is consistent with the data in Fig. 3(a). In addition, theory predicts that the thermal peaks will assume a maximum as a function of normal-state conductance. We observe such a maximum only for β_+. For β_-, the peak is expected to occur only at rather large normal-state conductance where our approximations of neglecting multiple Andreev reflections and a peak width smaller than ϵ_0 break down.

To further substantiate our analysis, we have used Eqs. (1) and (2) to fit all four peaks $\alpha_\pm$ and $\beta_\pm$ over the entire range of tunneling strengths; see Fig. 3(a) in the Supplemental Material [28]. There is excellent agreement between theory and experiment. We attribute the deviations for β_- at large normal-state conductance to additional contributions from multiple Andreev reflections. We can also extract the normal-state conductance at which the Andreev and single-particle contributions to the main peaks become comparable; see the arrows in Fig. 3(a). (Note that this is distinct from the crossover between linear and sublinear dependence.) For α_+, this happens when $2\Gamma_h(2\epsilon_0) \sim \Gamma_1$, and for α_-, when $2\Gamma_e(2\epsilon_0) \sim \Gamma_1$. As $v^2 > u^2$, the Andreev contribution sets in considerably earlier for α_+ than for α_-.

Relaxation rates.—At $T = 4.8$ K, the relaxation rate can be extracted directly from the peak width, yielding $\Gamma_1 \simeq 6$ ps. In contrast, the linewidth is resolution limited at $T = 1.2$ K, masking the broadening due to quasiparticle relaxation. We can still extract the relaxation rate by relying on the current. In the sublinear regime, the thermal peak β_+ contributes a current $I \sim e\Gamma_2/\hbar$ [28]. Moreover, Eq. (3) predicts $\Gamma_1 = (\alpha_+/\beta_-)\Gamma_2$ in the linear regime. Thus, we can extract both relaxation rates directly from the experimental data. This yields (to about a factor of 2) $\hbar/\Gamma_1 \simeq 0.2$ ns and $\hbar/\Gamma_2 \simeq 0.6$ ns.

For magnetic impurities binding a single Shiba state, relaxation relies on quasiparticle excitation to the continuum. This yields a ratio of relaxation rates at the two experimental temperatures of order $\sim 10^4$. We can account for the apparent discrepancy with our observations by including the second Shiba state at energy $\epsilon_1 \simeq 0.77$ meV. Then, relaxation can occur via the formation of Cooper pairs from quasiparticles in the first two Shiba states. This process is limited by the thermal occupation of the second Shiba state and thus involves a much smaller activation energy. Such processes are allowed even for Shiba states with equal spin due to the strong spin-orbit coupling of Pb. An analysis in terms of rate equations is quantitatively consistent with our observations [28].

Conclusions.—We show that STM experiments on subgap states in superconductors probe both single-electron and Andreev tunneling. We emphasize that such experiments are particularly fruitful when performed with superconducting tips. In this case, thermal smearing can be

neglected and the temperature dependence of the current arises entirely from activated quasiparticle relaxation processes. Moreover, the additional thermal peaks facilitate the analysis and provide access to the relaxation rates. We find that at weak tip-substrate tunneling, the current is dominated by single-electron tunneling and is linear in the normal-state conductance. This regime can be used to map out the bound-state wave function. At stronger tip-substrate tunneling, the dependence on the normal-state conductance becomes sublinear. While the dependence on the Shiba wave function becomes more involved, this regime provides access to pertinent quasiparticle relaxation rates involving the subgap states. Specifically, we can extract the rates for quasiparticle relaxation into and out of the bound state. The present experiment was restricted to two different temperatures. To further probe the microscopic nature of the relaxation processes, it would be rewarding to perform more systematic experiments as a function of temperature.

We thank Piet Brouwer and Leonid Glazman for discussions, and we acknowledge financial support by the Deutsche Forschungsgemeinschaft through the collaborative research center SFB 658 and Grant No. FR2726/4 (K. F.) as well as research priority programmes SPP 1285 and SPP 1666 (F. v. O.), by a Consolidator Grant from the European Research Council "NanoSpin" (K. F.), and by the Helmholtz Virtual Institute "New States of Matter and Their Excitations" (F. v. O.).

[1] A. V. Balatsky, I. Vekhter, and J.-X. Zhu, Rev. Mod. Phys. **78**, 373 (2006).
[2] A. Yazdani, B. A. Jones, C. P. Lutz, M. F. Crommie, and D. M. Eigler, Science **275**, 1767 (1997).
[3] A. Yazdani, C. M. Howald, C. P. Lutz, A. Kapitulnik, and D. M. Eigler, Phys. Rev. Lett. **83**, 176 (1999).
[4] L. Yu, Acta Phys. Sin. **21**, 75 (1965).
[5] H. Shiba, Prog. Theor. Phys. **40**, 435 (1968).
[6] A. I. Rusinov, Pis'ma Zh. Eksp. Teor. Fiz. **9**, 146 (1968) [JETP Lett. **9**, 85 (1969)].
[7] K. J. Franke, G. Schulze, and J. I. Pascual, Science **332**, 940 (2011).
[8] J. Bauer, J. I. Pascual, and K. J. Franke, Phys. Rev. B **87**, 075125 (2013).
[9] N. Y. Yao, C. P. Moca, I. Weymann, J. D. Sau, M. D. Lukin, E. A. Demler, and G. Zarand., Phys. Rev. B **90**, 241108(R) (2014).
[10] S. Nadj-Perge, I. K. Drozdov, B. A. Bernevig, and A. Yazdani, Phys. Rev. B **88**, 020407(R) (2013).
[11] F. Pientka, L. I. Glazman, and F. von Oppen, Phys. Rev. B **88**, 155420 (2013).
[12] J. Klinovaja, P. Stano, A. Yazdani, and D. Loss, Phys. Rev. Lett. **111**, 186805 (2013).
[13] S. Nadj-Perge, I. K. Drozdov, J. Li, H. Chen, S. Jeon, J. Seo, A. H. MacDonald, B. A. Bernevig, and A. Yazdani, Science **346**, 602 (2014).
[14] S.-H. Ji, T. Zhang, Y.-S. Fu, X. Chen, X.-C. Ma, J. Li, W.-H. Duan, J.-F. Jia, and Q.-K. Xue, Phys. Rev. Lett. **100**, 226801 (2008).
[15] A. Levy Yeyati, J. C. Cuevas, A. López-Dávalos, and A. Martín-Rodero, Phys. Rev. B **55**, R6137(R) (1997).
[16] B. M. Andersen, K. Flensberg, V. Koerting, and J. Paaske, Phys. Rev. Lett. **107**, 256802 (2011).
[17] P. A. Ioselevich and M. V. Feigelman, New J. Phys. **15**, 055011 (2013).
[18] I. Martin and D. Mozyrsky, Phys. Rev. B **90**, 100508 (2014).
[19] M. E. Flatté and J. M. Byers, Phys. Rev. Lett. **78**, 3761 (1997).
[20] M. I. Salkola, A. V. Balatsky, and J. R. Schrieffer, Phys. Rev. B **55**, 12648 (1997).
[21] M. R. Buitelaar, T. Nussbaumer, and C. Schönenberger, Phys. Rev. Lett. **89**, 256801 (2002).
[22] S. De Franceschi, L. Kouwenhoven, C. Schönenberger, and W. Wernsdorfer, Nat. Nanotechnol. **5**, 703 (2010).
[23] A. P. Higginbotham, S. M. Albrecht, G. Kirsanskas, W. Chang, F. Kuemmeth, P. Krogstrup, T. S. Jespersen, J. Nygard, K. Flensberg, and C. M. Marcus, arXiv:1501.05155.
[24] L. Bretheau, C. Ö. Girit, H. Pothier, D. Esteve, and C. Urbina, Nature (London) **499**, 312 (2013).
[25] F. Kos, S. E. Nigg, and L. I. Glazman, Phys. Rev. B **87**, 174521 (2013).
[26] D. G. Olivares, A. Levy Yeyati, L. Bretheau, C. Ö. Girit, H. Pothier, and C. Urbina, Phys. Rev. B **89**, 104504 (2014).
[27] A. G. Kozorezov, A. A. Golubov, J. K. Wigmore, D. Martin, P. Verhoeve, R. A. Hijmering, and I. Jerjen, Phys. Rev. B **78**, 174501 (2008).
[28] See Supplemental Material at http://link.aps.org/supplemental/10.1103/PhysRevLett.115.087001, which includes Ref. [29], for more experimental data, a self-contained description of the theoretical analysis, and details of the theoretical interpretation of the experimental data.
[29] D. A. Ivanov and M. V. Feigel'man, JETP Lett. **68**, 890 (1998).
[30] B. W. Heinrich, L. Braun, J. I. Pascual, and K. J. Franke, Nat. Phys. **9**, 765 (2013).
[31] M. Ruby, B. W. Heinrich, J. I. Pascual, and K. J. Franke, Phys. Rev. Lett. **114**, 157001 (2015).
[32] At small tip-sample distances, weak additional resonances appear due to dc Josephson currents and multiple Andreev reflections.
[33] M. Ternes, W.-D. Schneider, J. C. Cuevas, C. P. Lutz, C. F. Hirjibehedin, and A. J. Heinrich, Phys. Rev. B **74**, 132501 (2006).
[34] C. P. Moca, E. Demler, B. Jankó, and G. Zaránd, Phys. Rev. B **77**, 174516 (2008).
[35] R. Zitko, O. Bodensiek, and T. Pruschke, Phys. Rev. B **83**, 054512 (2011).
[36] H. Haug and A.-P. Jauho, *Quantum Kinetics in Transport and Optics of Semiconductors* (Springer, New York, 2008).
[37] J. C. Cuevas, A. Martín-Rodero, and A. Levy Yeyati, Phys. Rev. B **54**, 7366 (1996).
[38] C. Berthod and T. Giamarchi, Phys. Rev. B **84**, 155414 (2011).
[39] D. Averin and A. Bardas, Phys. Rev. Lett. **75**, 1831 (1995).